Time Dependent Electric Fields Generated DC Currents in a Large Gate-Defined Open Dot

2010 Jpn. J. Appl. Phys. 49 114001

(http://iopscience.iop.org/1347-4065/49/11R/114001)

Time Dependent Electric Fields Generated DC Currents in a Large Gate-Defined Open Dot

Kai-Ming Liu*, Vladimir Umansky[1], and Shih-Ying Hsu

Department of Electrophysics, National Chiao Tung University, Hsinchu 30010, Taiwan
[1]*Braun Center for Submicron Research, Weizmann Institute of Science, Rehovot 76100, Israel*

Received June 23, 2010; accepted September 4, 2010; published online November 22, 2010

We present the study of DC currents of an open dot generated from two time dependent electric fields in the absence of external bias. Two electrical setups were applied. In one configuration, two fast oscillating voltages were applied on two side gates; in the other, one of the oscillating biases was directly applied to the source lead. The DC current as a function of frequency, coupling strength, and magnetic field was investigated. The current is sinusoidally dependent with the phase shift and bilinearly dependent with the excitation voltage for both configurations. However, the current as a function of frequency, coupling strength, and magnetic fields behaves differently in these two setups. The results indicate that the currents generated in different setups originate from different mechanisms, and moreover, not from any classical circuitry effect.

DOI: 10.1143/JJAP.49.114001

1. Introduction

The recent realization of charge pump in mesoscopic devices is the capability of converting time-dependent signals to DC signals. By a variety of ways, such as cyclically deforming two system parameters of a quantum dot,[1)] a quantum wire[2)] or an interdigitated ratchet on the two-dimensional electron gas (2DEG),[3,4)] a DC current is produced without external voltage bias. It has been well known that traveling potentials generated by surface acoustic wave in GaAs/AlGaAs heterostructures also result in DC response.[5,6)] These techniques may be useful, since such transformations may be used for the operations of power rectification and signal processing in integrated circuits[7)] or signal modulation in telecommunications.[8)] The idea of charge pump is particularly fascinating among these techniques, because the current would be dissipationless, i.e., the power consumption would be infinitesimal.[9–11)] However, the experimental fulfillment is challenging and the evidence is much more subtle. There may be other effects that could mix with quantum pumping. Rectification, induced from coupling between time-varying conductance and chemical potentials of reservoirs of a quantum dot, is one most possible candidate.[12–14)] Therefore, it is important to understand comprehensively those interfering effects prior to the practical applications of the AC–DC transformation in nano-scaled semiconductor devices.

In this work, we study the performance of generated DC current I_{dc} by two fast oscillating electric fields in an open dot for two different electrical configurations. In the first setup, the AC voltages are applied on two side gates resembling the typical charge pump; in the other, one AC voltage is relocated to the source lead being similar to the condition of rectification. Both setups demonstrate that I_{dc} depends sinusoidally on the phase difference between the two AC voltages, $\Delta\phi$. Additionally, I_{dc} is proportional to the product of the two voltage amplitudes. However, the dependences of I_{dc} on frequency, coupling strength, and magnetic field in both setups show the opposite features. The results indicate that the currents are generated by different mechanisms, however, not by any classical circuitry effect. The results also suggest that the current generated in the pump-like setup is a type of charge pump.

*E-mail address: arthurliu.ep91g@nctu.edu.tw

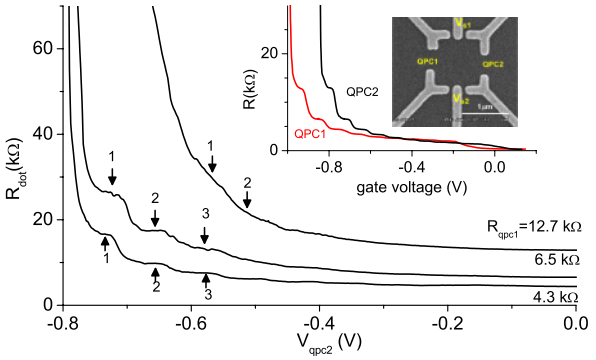

Fig. 1. (Color online) Dot resistance as a function of gate voltage V_{qpc2} when QPC1 is confined at 4.3, 6.5, and 12.7 kΩ. The mode number of QPC1, N_{qpc1}, is 3, 2, and 1, respectively. The mode number of QPC2 is counted and labeled on the trace by the numbers. Inset: SEM image of the device and resistance of one QPC vs gate voltage when the other QPC is applied by a small positive voltage. The left (red) and right (black) traces are for QPC1 and QPC2, respectively.

2. Experiments

The 2DEG forms at the interface of a GaAs/Al_xGa_{1-x}As heterostructure. The 2DEG is ~93 nm beneath the substrate surface. Shubnikov-de Haas and Hall measurements were used to determine the bulk electron density n and mobility. Mobility is about 1.7×10^6 cm^2 V^{-1} s^{-1} at low temperatures and n is 2.4×10^{11} cm^{-2} corresponding to an elastic mean free path of ~14 μm. Electron beam lithography was used to pattern the surface of GaAs/Al_xGa_{1-x}As heterostructure with numerous geometrical arrangements. As shown in the inset of Fig. 1, there are four corner gates to confine an area with two quantum point contacts (QPCs) serving as the entrance and exit to the reservoirs. The gap width of the QPCs are ~0.4 μm. The other two gaps where the side gates, s1 and s2, are lying in between have a width of ~0.35 μm. This design ensures that when both QPCs are confined, constrictions are also developed at the two side gaps. When the voltage excitations are applied to the side gates, the induced potentials superimpose on the confinement created by other four gates, being able to disturb the electrons inside the confined dot. The lithographic area of the dot is about 1 μm^2 resulting in an average level spacing $\Delta = 2\pi\hbar^2/m^*A \sim 7.2$ μeV. The electron number is estimated to be

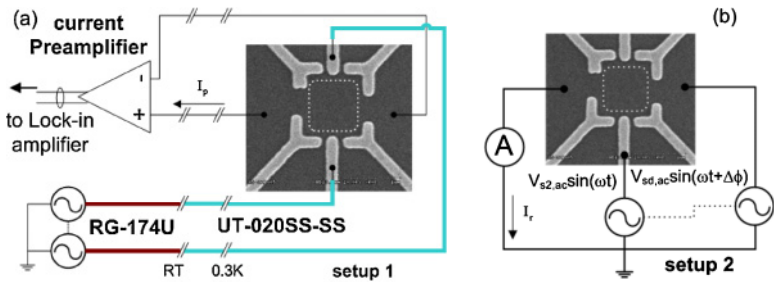

Fig. 2. (Color online) (a) Circuit diagram of the electrical setup 1. Both AC voltages are applied to middle side gates. (b) A simplified sketch of setup 2. One AC voltage is applied to the source lead.

~2000 in the dot. Experiments were carried out in a pumped ^{3}He refrigerator with a base temperature of 0.28 K. Data presented here was taken at 0.3 K.

The resistance of a quantum point contact shows clear steps as a function of gate voltage $V_{qpc1(2)}$ as shown in the inset of Fig. 1. The resistance is quantized at $1/i(h/2e^2) = 12.9\,\mathrm{k\Omega}/i$, where $i = 1, 2, \ldots$, indicating a well defined transmission mode in the QPCs. Figure 1 shows the resistance when both QPCs are confined and the large dot is developed. To systematically characterize the mode number N of the confined open dot, V_{qpc1} was first fixed at a certain plateau then V_{qpc2} was swept. For example, V_{qpc1} is fixed at the 4.3 kΩ plateau, referring to a mode number of three in QPC1. (The lowest trace in the figure.) The dot resistance R_{dot} increases with decreasing V_{qpc2} revealing several steps along the trace. The mode number of QPC2 in the dot is determined by counting the steps from the pinch-off. For the step labeled "1", the resistance is about 16.7 kΩ when the dot has a mode number $N = (N_{qpc1}, N_{qpc2}) = (3, 1)$. In the trace of $R_{qpc1} = 12.7\,\mathrm{k\Omega}$ (or $N_{qpc1} = 1$), the resistance plateaus are more smooth but still discernible. The steps have a resistance larger than the addition of the separate QPCs' resistances. Step "1" is about 30 kΩ for $N = (1, 1)$ while step "2" is about 21 kΩ for $N = (1, 2)$.

In setup 1 which resembles the typical charge pump,[9,15] two fast oscillating voltages with the same frequency ($f \sim 0.1$–10 MHz) were applied to the two side gates. $V_{s1}(t) = V_{s1,ac}\sin(\omega t + \Delta\phi)$ and $V_{s2}(t) = V_{s2,ac}\sin(\omega t)$. As shown in Fig. 2(a), the signals were fed through coaxial cables in the fridge with the nominal attenuation of 12.7 dB/m at 0.5 GHz and 18.7 dB/m at 1 GHz. By separate measurements, the attenuation in our system for the applied frequencies were calibrated. Loss is ~6.8 dB at 10 MHz from the signal generators to the sample in the fridge. To allow a sensitive lock-in measurement, the signals from the signal generators were chopped by a low frequency square wave at 101 Hz. The DC current I_p, was amplified by a current preamplifier before being input to the lock-in amplifier. The measurement methods in setup 2 are the same as in setup 1, except one oscillating voltage was applied to the source lead as shown in Fig. 2(b). The conductance of the dot is expected to oscillate as a function of time corresponding to the oscillating side gate voltage, as well as the source lead chemical potential. The setup resembles the rectification effect.[12] The generated current I_r is expected to flow to the ground passing the current preamplifier. These two signal generators were synchronized with a phase difference $\Delta\phi$ between them.

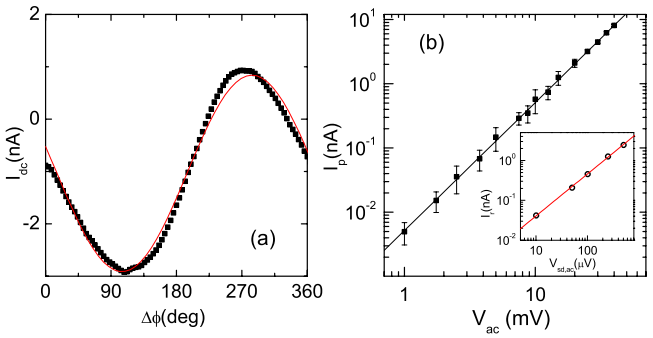

Fig. 3. (Color online) (a) Typical plot of the measured $I_{dc}(\Delta\phi)$ [points] along with the fit of the form $I_{dc}(\Delta\phi) = I_{p(r)}\sin(\Delta\phi + \phi_0) + I_0$ [solid curve]. (b) Logarithmic plot of $I_p(V_{ac})$ with a power law fit (solid line). The least square root fit gives a power of 1.99 ± 0.06. The channel number of both entrance and exit of the dot is controlled to be two and the frequency of the AC voltage is 7 MHz. Inset: logarithmic plot of $I_r(V_{sd,ac})$ for $N = (2, 2)$, $f = 5$ MHz, and $V_{s2,ac} = 15$ mV for setup 2. The solid line is the least square root fit of power law.

3. Results and Discussion

Scattered points in Fig. 3(a) are the typical result of the measured DC current as a function of the phase difference. I_{dc} as a function of $\Delta\phi$ has the sinusoidal form with a small offset in a period of 2π. To systematically characterize the current amplitude, data is numerically fit with the form $I_{dc}(\Delta\phi) = I_{p(r)}\sin(\Delta\phi + \phi_0) + I_0$. The solid line in the panel is the fit to data by least square root regression. The current generated in setup 1 I_p as a function of voltage amplitude for $N = (2, 2)$ and $f = 7$ MHz is presented in Fig. 3(b). Equal voltage amplitude is applied on both side gates, i.e., $V_{s1,ac} = V_{s2,ac} = V_{ac}$. In this logarithmic plot, the data points follow a straight line of slope of 2 indicating a bilinear dependence $I_p \propto (V_{ac})^2$. I_p increases from as low as tens of pA for $V_{ac} = 1$ mV to tens of nA for $V_{ac} = 40$ mV. For $V_{ac} > 40$ mV, nonlinear effect becomes significant and $I_{dc}(\Delta\phi)$ becomes non-sinusoidal. Inset of Fig. 3(b) shows the current generated in setup 2 as a function of the AC source voltage $I_r(V_{sd,ac}, V_{s2,ac} = 15\,\mathrm{mV})$ for $N = (2, 2)$ and $f = 5$ MHz. The slope of the trace is ~1.05, also implying a bilinear dependence on the voltage amplitudes for the DC current.

Although the phase difference and amplitude dependences of I_p and I_r are similar, their dependences on frequency, coupling strength, and magnetic fields are contrastive. In Fig. 4(a), the five datasets demonstrate the relation between I_p and frequency for various coupling strengths between the dot and the reservoirs. From top down, the mode number of

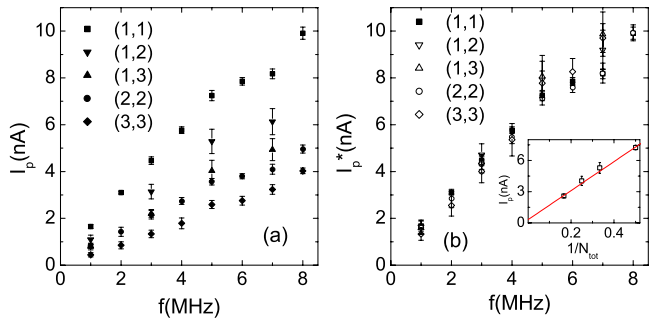

Fig. 4. (Color online) (a) DC current generated in setup 1, I_p, as a function of frequency for an open dot of different transmission mode numbers in QPC1 and QPC2. Each data point is averaged over five datasets of $I_{dc}(\Delta\phi)$. The legend indicates the transmission mode number N of the dot. $V_{ac} = 15\,\mathrm{mV}$. (b) Rescaled current I_p^* vs f for the same mode numbers. $I_p^*(N) = [(N_{qpc1} + N_{qpc2})/2]I_p(N)$. I_p of $N = (1,2)$, $(1,3)$, $(2,2)$, and $(3,3)$ are multiplied by the total mode number ratio with respect to $N = (1,1)$. Inset: I_p vs $(N_{tot})^{-1}$ for 5 MHz. The solid line is the linear fit by least-square-root-regression.

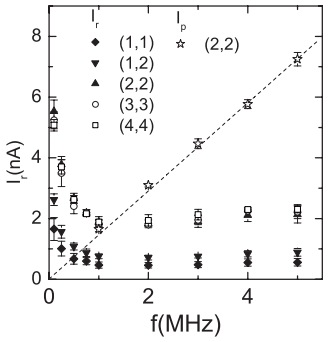

Fig. 5. DC current I_r in setup 2 as a function of frequency for various mode numbers. The legend indicates the corresponding mode number of the dot. $V_{sd,ac} = 1\,\mathrm{mV}$ and $V_{s2,ac} = 25\,\mathrm{mV}$. For comparison, $I_p(f)$ for $V_{ac} = 15\,\mathrm{mV}$ and $N = (2,2)$ (☆) is also plotted. The straight dashed line is the visual guide.

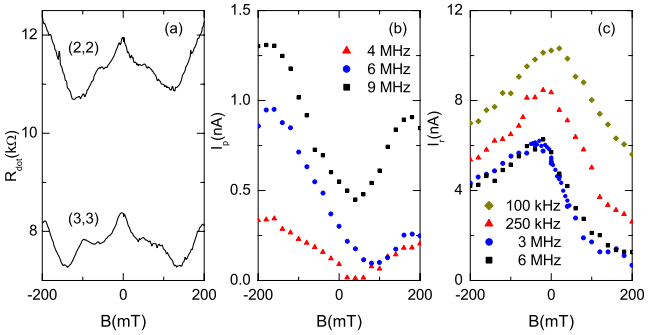

Fig. 6. (Color online) (a) Dot resistance as a function of perpendicular magnetic field for $N = (2,2)$ [top] and $(3,3)$ [bottom], respectively. (b) I_p vs B for three frequencies at $N = (2,2)$. The legend indicates the frequency. (c) I_r vs B for four frequencies at $N = (3,3)$.

QPC1 and QPC2 are $(1,1)$, $(1,2)$, $(1,3)$, and so on. I_p is about linearly dependent with the frequency for $f \lesssim 8\,\mathrm{MHz}$. The current begins to saturate for higher frequencies. The DC current is the largest for $N = (1,1)$ and decreases with increasing mode number. There is one thing worth to be mentioned: I_p drops rapidly as soon as the dot is closed when R_{dot} is slightly larger than e^2/h corresponding to $N = (0,0)$. Although the measured R_{dot} is still finite $\sim 100\,\mathrm{k\Omega}$, the measured current reduces to almost beyond the experimental resolution. Interestingly, I_p is found to follow a specific relation with the total mode number of the dot $N_{tot} = N_{qpc1} + N_{qpc2}$. The ratio of N_{tot} for the last four datasets to $N = (1,1)$ is $3/2$, 2, 2, and 3, respectively. Figure 4(b) shows the rescaled I_p being multiplied by the ratio, for example, $I_p^*[N = (1,2)] = 3/2 \cdot I_p[N = (1,2)]$. All datasets normalized to the $N = (1,1)$ trace fall onto one trace. I_p not only decreases with increasing N_{tot} (or the increasing coupling strength between the dot and reservoirs), but is also proportional to $(N_{tot})^{-1}$ as demonstrated in the inset of Fig. 4(b). The results imply that the generated current is a type of charge pump as argued in the following. (1) The escape rate Γ_{esc} of electrons in an open quantum dot is determined by the total channel number N_{tot} and follows $\Gamma_{esc} \sim N_{tot}\Delta/2\pi^2$. The escaping or leaking of electrons from the dot increases with increasing coupling strength which also reduces the time that electrons relax to the reservoirs. Therefore, one would expect the performance of pumping to be suppressed by the increased coupling strength due to the opening of the dot,[16–19] or the dephasing due to the inelastic scattering from a third fictitious voltage probe.[20] (2) If the current is a result of any circuitry effect (for example, classical dependence of the resistance on the applied electric fields or cross talk between the electric signals), I_p would increase monotonically with increasing dot resistance regardless of the mode number N, and $I_p[N = (0,0)]$ should be greater than $I_p[N = (1,1)]$. But this scenario does not apply to our results.

The current generated in setup 2 has completely different characteristics. As shown in Fig. 5, I_r decreases with increasing frequency for $f \sim 0.1$–$1\,\mathrm{MHz}$, and then increases very slightly from 1 to 5 MHz for various mode numbers. For comparison, $I_p(f)$ for $N = (2,2)$ is also presented in the same plot as the starry points. I_r has a very dissimilar frequency dependence compared with I_p. In addition, as opposed to setup 1, I_r is the smallest for $N = (1,1)$ at a fixed frequency, increases with N, and saturates at higher mode number for $N \geqslant (3,3)$. No specific relation between the current and the mode number is found. In this setup, the source–drain voltage $V_{sd}(t)$ and the dot conductance $G(t) = [R_{dot}(t)]^{-1}$ are expected to oscillate with the same frequency. Similar to the rectification mechanism, the current $I_r = (\omega/2\pi)\int_0^{2\pi/\omega} V_{sd}(t)G[V_{s2}(t)]\,dt$, where $V_{sd}(t) = V_{sd,ac}\sin(\omega t + \Delta\phi)$ and $V_{s2}(t) = V_{s2,ac}(\omega t)$. For a small driving amplitude, $G[V_{s2}(t)] \approx G + (\partial G/\partial V_{s2})\delta V_{s2}$ and $I_r \approx V_{sd,ac}V_{s2,ac}(\partial G/\partial V_{s2})(\cos\phi/2)$, independent of ω. As shown in Fig. 5, I_r has a rarely slow response to f compared with I_p for $1\,\mathrm{MHz} < f < 6\,\mathrm{MHz}$. Besides, the rate of the increase in I_r with respect to f is almost the same for different transmission modes N.

To further investigate the characteristics of the two DC currents, transport in perpendicular magnetic fields B was also studied. The magnetic field is normal to the plane of the 2DEG. The dot resistance as a function of B is presented in Fig. 6(a) for $N = (2,2)$ and $(3,3)$, respectively. Both traces are as a whole symmetric in magnetic field. R_{dot} decreases with increasing B due to weak localization effect for $|B| \lesssim 130\,\mathrm{mT}$.[21,22] R_{dot} decreases from $\sim 12\,\mathrm{k\Omega}$ at $B = 0$ to $\sim 10.8\,\mathrm{k\Omega}$ for $N = (2,2)$ and from $\sim 8.4\,\mathrm{k\Omega}$ at $B = 0$ to

$\sim$7.3 kΩ for $N = (3, 3)$. The resistance increases then with increasing magnetic field for $|B| \gtrsim 130$ mT. Figures 6(b)–6(c) show the magnetic field dependence of I_p and I_r for various frequencies. Compared with Fig. 6(a), it is evident that $I_p(B)$ and $I_r(B)$ are uncorrelated with $R_{dot}(B)$. Additionally, I_r becomes asymmetric with respect to B with increasing frequency while the magnetoresistance of the dot is symmetric about B. In Fig. 6(c), the trace for 3 MHz is more asymmetric than 100 kHz. The results again suggest that there is no possibility of circuitry effect for both DC currents. As far as the classical circuitry effect is concerned, a DC current could be measured when a DC voltage drop is created across the dot. The Ti/Au Schottky gates form effectively a metal-semiconductor junction similar to a p–n junction which could rectify the applied AC voltage to create a DC bias on the source lead. Regarding the confined open dot as a classical resistor, a DC current would be produced by the DC bias. However, this effect can be excluded since the applied AC voltage is smaller than 40 mV, well below the threshold voltage of $\sim$+0.6 V for the Schottky contact. On the other hand, the magnetic field dependence of the current show discrepancies in I_p and I_r. I_p overall increases but I_r decreases with increasing $|B|$. This difference further support that I_p and I_r are indeed generated by different mechanisms.

4. Conclusions

In conclusion, DC currents in an open dot are generated from two time dependent electric fields in two electrical setups. The currents show different dependences on frequency, mode number, and perpendicular magnetic field. I_p increases linearly with increasing frequency for $f \lesssim 8$ MHz. It decreases with the total mode number in the relation of $I_p \propto (N_{qpc1} + N_{pqc2})^{-1}$, which may be attributed to the relaxation of the electrons from the dot. As soon as the entrance and exit of the dot are almost closed with less than one transmission mode number while the resistance is still finite, I_p drops rapidly almost beyond the experimental resolution. I_p on the whole increases with increasing magnetic field. On the contrary, I_r decreases with increasing f and becomes insensitive to frequency for $f \gtrsim 1$ MHz. It increases with increasing the mode number, and saturates at higher mode numbers for $N \geqslant (3, 3)$. I_r decreases with increasing $|B|$. Moreover, both $I_p(B)$ and $I_r(B)$ can be asymmetric in magnetic field but have no direct correlation with the dot resistance $R_{dot}(B)$. We believe that the classical circuitry effects can be ruled out for the current generation. Our results suggest that I_p and I_r are indeed originated from different mechanisms and these two types of current can be distinguished by the details of electrical configurations.

Acknowledgments

We appreciate precious discussions with C. S. Chu, Y. W. Suen, C. S. Tang, and M. Moskalets. This work was supported by NSC grant in Taiwan under project No. NSC96-2112-M-009-030-MY3 and MOE ATU program.

1) M. Switkes, C. Marcus, K. Campman, and A. Gossard: Science **283** (1999) 1905.
2) M. D. Blumenthal, B. Kaestner, L. Li, S. Giblin, T. J. B. M. Janssen, M. Pepper, D. Anderson, G. Jones, and D. A. Ritchie: Nat. Phys. **3** (2007) 343.
3) E. M. Höhberger, A. Lorke, W. Wegscheider, and M. Bichler: Appl. Phys. Lett. **78** (2001) 2905.
4) T. Müller, A. Würtz, A. Lorke, D. Reuter, and A. D. Wieck: Appl. Phys. Lett. **87** (2005) 042104.
5) V. I. Talyanskii, J. M. Shilton, M. Pepper, C. G. Smith, C. J. B. Ford, E. H. Linfield, D. A. Ritchie, and G. A. C. Jones: Phys. Rev. B **56** (1997) 15180.
6) J. Ebbecke, N. E. Fletcher, T. J. B. M. Janssen, F. J. Ahlers, M. Pepper, H. E. Beere, and D. A. Ritchie: Appl. Phys. Lett. **84** (2004) 4319.
7) A. S. Sedra and K. C. Smith: *Microelectronic Circuits* (Oxford University Press, New York, 2004) Chap. 3.
8) R. E. Ziemer and W. H. Tranter: *Principles of Communications* (Wiley, New York, 1995) Chap. 3.
9) P. W. Brouwer: Phys. Rev. B **58** (1998) R10135.
10) M. Büttiker, H. Thomas, and A. Pretre: Z. Phys. B **94** (1994) 133.
11) F. Zhou, B. Spivak, and B. Altshuler: Phys. Rev. Lett. **82** (1999) 608.
12) P. W. Brouwer: Phys. Rev. B **63** (2001) 121303.
13) L. DiCarlo, C. M. Marcus, and J. S. Harris: Phys. Rev. Lett. **91** (2003) 246804.
14) M. G. Vavilov, L. DiCarlo, and C. M. Marcus: Phys. Rev. B **71** (2005) 241309.
15) B. L. Altshuler and L. I. Glazman: Science **283** (1999) 1864.
16) J. N. H. J. Cremers and P. W. Brouwer: Phys. Rev. B **65** (2002) 115333.
17) C. S. Tang, Y. H. Tan, and C. S. Chu: Phys. Rev. B **67** (2003) 205324.
18) E. Faizabadi and F. Ebrahimi: J. Phys.: Condens. Matter **16** (2004) 1789.
19) S. Banerjee, A. Mukherjee, S. Rao, and A. Saha: Phys. Rev. B **75** (2007) 153407.
20) M. Moskalets and M. Büttiker: Phys. Rev. B **64** (2001) 201305.
21) A. M. Chang, H. U. Baranger, L. N. Pfeiffer, and K. W. West: Phys. Rev. Lett. **73** (1994) 2111.
22) A. G. Huibers, M. Switkes, C. M. Marcus, K. Campman, and A. C. Gossard: Phys. Rev. Lett. **81** (1998) 200.